SQUID MEASUREMENT OF METALLOPROTEIN MAGNETIZATION

New Methods Applied to the Nitrogenase Proteins

EDMUND P. DAY,* THOMAS A. KENT,* PAUL A. LINDAHL,‡ ECKARD MÜNCK,*
WILLIAM H. ORME-JOHNSON,‡ HEINRICH RODER,§ AND A. ROY§
*Gray Freshwater Biological Institute, University of Minnesota, Navarre, Minnesota 55392;
‡Chemistry Department, Massachusetts Institute of Technology, Cambridge, Massachusetts 02139;
§ Department of Physics, University of Illinois at Urbana-Champaign, Urbana, Illinois 61801

ABSTRACT New techniques have been developed to exploit the sensitivity of a commercial SQUID susceptometer in the study of the magnetization of metalloproteins. Previous studies have ignored both the slow relaxation (hours) of spin $I = \frac{1}{2}$ nuclei and residual ferromagnetic impurities in sample holders. These potential sources of noise were at or below the sensitivity of previous instruments. With these noise sources under control, one can now decrease the protein concentration by a factor of ten. In addition careful characterization of the frozen magnetization sample, including the use of a multi-instrument holder for combined study of the magnetization sample with Mössbauer spectroscopy, is required for reliable interpretation of the data in the face of paramagnetic impurities common to metalloprotein samples. Many previous magnetic studies of metalloproteins have been carried out in the Curie region. Saturation magnetization studies down to 1.8 K and up to 5 T can determine zero-field splitting parameters in addition to the spin and exchange coupling parameters measured in previous studies at lower fields and higher temperatures. Applications of these techniques to the study of the nitrogenase proteins of *Azotobacter vinelandii* are presented as examples.

I. INTRODUCTION

This paper describes techniques developed for magnetization studies of metalloproteins using a commercial SQUID susceptometer (Biomagnetic Technologies, Inc. [BTi], San Diego, CA). Several of these techniques overcome fundamental problems in the study of weakly magnetic materials and should be of general use in any study that exploits the full sensitivity of the SQUID susceptometer. Two examples drawn from our nitrogenase research are included to illustrate the new techniques.

In the past, noise sources within the sample and instrument insensitivity have limited metalloprotein magnetization measurements to highly concentrated[1] (>3 mM) samples (see Table I). The improved sensitivity of commercial SQUID susceptometers combined with the techniques to be described here makes it possible to study the saturation magnetization of small volume (<0.2 ml), low concentration[1] (<0.3 mM) metalloprotein samples. Besides the obvious advantage of requiring less protein, the lower concentration makes possible the study of high molecular weight proteins which are difficult to concentrate to the millimolar level. The MoFe-protein of nitrogenase with a molecular weight of 240,000 is presented below as an example.

A magnetization measurement detects the sum of contributions from the metalloprotein, buffer, and sample holder. The paramagnetic signal of interest is often small compared with the diamagnetism. The large diamagnetic background (which is independent of temperature and linear in magnetic field) is removed by subtracting the signal of a matched control from that of the metalloprotein sample.

With the improved sensitivity of the commercial SQUID susceptometer, ferromagnetic (or superparamagnetic) impurities in the sample holder become a significant problem. The magnetization of ferromagnetic impurities can be separated from the paramagnetic signal of interest because it has a very different dependence on field and temperature.

The sensitivity of the SQUID susceptometer makes the

[1] These concentrations refer to a spin $S = \frac{1}{2}$ state. Higher spin states can be studied at lower concentrations. The magnetization signal is proportional to $S(S + 1)$ at high temperatures when the Curie law is obeyed.

Dr. Lindahl's present address is Gray Freshwater Biological Institute, University of Minnesota, P. O. Box 100, Navarre, MN 55392.

Dr. Roder's present address is Department of Biochemistry and Biophysics, University of Pennsylvania School of Medicine, Philadelphia, PA 19104.

Dr. Roy's present address is Department of Physics, City College of New York, Convent Avenue at 138th Street, New York, NY 10031.

detection of the nuclear spin magnetization of the protons in water (1) (or of the protons or fluorine nuclei in plastic sample holders) straightforward. Unfortunately this can lead to a lack of reproducibility in magnetization studies (2) due to the long relaxation time (hours) of spin $I = \frac{1}{2}$ nuclei in frozen samples (3). This noise source has been eliminated here by using deuterated buffers and by avoiding plastic sample holders. Deuteration introduces fast relaxing nuclear paramagnetism, which can be subtracted easily using a matched control.

Four different techniques for measuring metalloprotein susceptibility are compared in Table I. Included is a study (labeled SQUID susceptometer) using the techniques to be detailed here. The amount of protein used in each study is given in the fourth column, whereas the protein concentration is given in column five. These numbers have been scaled to facilitate comparison of the three different studies of the reduced two iron ferredoxins and the one study of the Fe protein of nitrogenase. The sixth column gives the signal to noise estimated from the appropriate figures in the cited references for the stated concentrations (fifth column) between the stated temperatures (third column). The seventh column gives the signal to noise normalized to a concentration of 1 mM spin $S = \frac{1}{2}$ electrons obeying the Curie law between 10 and 50 K. The first footnote of Table I summarizes several of the background signals to be discussed in this paper, which become increasingly important as the protein concentration is decreased.

The normalized signal to noise (seventh column) of Table I indicates that, in the measurement of metalloprotein magnetization, techniques using either the Faraday balance or the SQUID susceptometer can achieve comparable sensitivities. Note that when this sensitivity is combined with deuteration of the buffer and other techniques to be described here (fourth row) the total amount of protein (fourth column) is reduced fourfold and the required concentration (fifth column) is decreased sevenfold from that needed when protons are present (third row). It is also clear from Table I that the background signal due to oxygen (0.67 mM spin $S = \frac{1}{2}$ electrons) must be removed as the protein concentration drops below 7 mM. Moreover, the background signal due to the proton nuclear susceptibility (0.26 mM spin $S = \frac{1}{2}$ electrons) must be removed when the protein concentration is decreased below 3 mM.

Paramagnetic impurities in metalloprotein samples make reliable interpretation of magnetization data difficult. This problem has to do with sample purity and is unaffected by instrument sensitivity or the noise sources mentioned above. Minimizing impurities and then characterizing those that remain by using electron paramagnetic resonance (EPR) and Mössbauer spectroscopies is one way to deal with this problem (8). An essential technique we have developed is the use of a multi-instrument sample holder. This allows us to make measurements on the magnetization sample using Mössbauer spectroscopy with-

TABLE I
COMPARISON OF SUSCEPTIBILITY MEASUREMENTS OF METALLOPROTEINS

Technique	Sample	Temp. range	Norm. amount*	Norm. conc.*	Specific S/N‡	Norm. S/N§	Ref. No.
		min K, max K	*μmol*	*mM*			
Torsion balance	[2Fe – 2S] fd spinach	(77, 115)	19.0	15.8	10	12	4
Vibrating sample magnetometer	[2Fe – 2S] fd parsley spinach	(1.47, 201)	2.8	3.7	25	0.8	5
Faraday balance	[2Fe – 2S] fd algae	(40, 77)	0.86	8.1	37	30	6
SQUID susceptometer	Fe protein of nitrogenase in D_2O	(11, 67)	0.21	1.2	36	32	7

Background signals: The following is a partial list of potential contributions to an observed Curie law slope expressed as a concentration (mM) of spin $S = \frac{1}{2}$ electrons: Oxygen, (air-saturated H_2O at 30°C; $S = 1$ [250 $\mu M \times 8/3$]), 0.67; protons, (in H_2O) nuclear paramagnetism, 0.26; deuterons, (in D_2O) nuclear paramagnetism, 0.02; helium gas, (displaced ideal gas at one atmosphere pressure), 0.18. Ferromagnetic impurities in sample holder materials are a significant noise source, which is discussed in the text (see Figs. 5 and 6). This noise does not show up as a temperature-independent change in the Curie law slope as do the listed noise sources.

*The total amount and concentration of protein has been scaled in each case to normalize differences between the studies. The stated numbers reflect the amount and concentration of protein required to generate the observed signal assuming the sample to be entirely in a pure spin $S = \frac{1}{2}$ state. For example, the numbers in the first row have been multiplied by 1.35 because this particular sample had a 3% spin $S = \frac{1}{2}$ impurity in addition to the spin S = $\frac{1}{2}$ state of the protein.

‡The signal was measured from the appropriate figure in each reference as the change in susceptibility between the two stated temperatures (third column). The spin $S = \frac{1}{2}$ concentration generating this signal is stated in the fifth column of this table. The noise was estimated from the worst case point to point data at one temperature when more than one run was given or from the worst case deviation from the theoretical curve when only one run was given.

§These signals have been scaled to a concentration of 1 mM of spin $S = \frac{1}{2}$ electrons obeying the Curie law between the temperatures of 10 and 50 K.

out thawing the sample or changing its concentration or holder. This technique is used to verify the redox state of the sample in addition to measuring the amounts of common paramagnetic impurities. Iron impurities can usually be detected by Mössbauer (Fe^{2+}) and EPR (Fe^{3+}) while many other paramagnetic metal impurities can be detected by EPR (Cu^{2+}, Mn^{2+}, Co^{2+}, etc.). Plasma emission or atomic absorption spectroscopy can inform us of the presence of these and other metals. A redox study can determine the state of those metals that are present at concentrations high enough to influence the interpretation of the magnetization data. Our published study of the Fe-protein of nitrogenase (7) and new results for the MoFe-protein of nitrogenase will be discussed as examples of this approach.

A preferable technique for dealing with paramagnetic impurities is to trigger the magnetization change of interest and to study the difference induced by the trigger. Any impurities unaffected by the trigger will be subtracted. Injection of CO can often be used, for example, to change a spin $S = 2$ state of a reduced hemeprotein to spin $S = 0$. Alternatively the reverse magnetization change can be photo-induced at low temperatures with the sample in the SQUID susceptometer. These techniques have been used in a study of myoglobin (9).

Saturation magnetization data provide a better test of theoretical models than susceptibility data limited to the Curie law region. A metalloprotein sample can now routinely be studied with a commercial SQUID susceptometer at temperatures down to 1.8 K and at fields up to 5 T. This increases the volume of thermodynamic phase space being explored over that of many previous metalloprotein studies. There are two particularly informative saturation magnetization curves: (*a*) the isofield curve at the highest achievable field (5 T), and (*b*) the isotherm curve at the lowest achievable temperature (1.8 K).

The shapes alone of these two saturation curves can often be used to determine the dominant spin of the sample. In favorable circumstances involving a homogeneous redox state with few impurities, these curves can be used to determine the concentration, spin, and zero-field splittings (including the sign and magnitude of D and the magnitude of E) of the metalloprotein paramagnetism.

II. PRINCIPLES OF SQUID MAGNETIZATION MEASUREMENTS

The essential features of a SQUID susceptometer (10) are indicated schematically in Fig. 1. Changes in magnetic flux are detected by the instrument's pickup coil system, which consists of a closed superconducting loop. Magnetic flux threading this loop is quantized and conserved. The flux change caused by sample insertion into the upper detection coil, for example, will induce a persistent current whose associated flux will exactly cancel the change. The result is zero change in the net flux threading the entire circuit with an accompanying change in the local flux at the SQUID detector that is proportional to the sample's magnetization. The SQUID signal is given as a function of sample position in Fig. 1. The circuit's response is immediate[2] and persists as long as the circuit is maintained in the superconducting state.

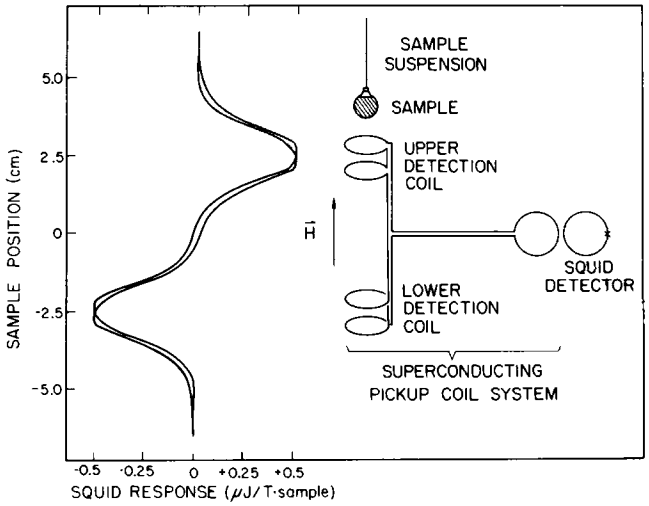

FIGURE 1 Sample insertion signal (*left*) and schematic diagram of a SQUID susceptometer (*right*). The left of the figure presents a recorder trace of the SQUID response as a sample of D_2O (0.10 ml) in a sealed quartz bulb (0.20 g) was moved vertically at a rate of 20 cm/min from above the upper detection coil through the two detection coils and back. The field was 1 T and the temperature was 5 K. The peak to peak SQUID reading corresponds to a sample magnetization of 0.994 μJ/T sample. There is hysteresis in the trace with the sample moving as it is here at the instrument's maximum speed of 20 cm/min. This was the insertion rate used by the manufacturer in calibrating the instrument. The same insertion rate was used throughout these studies. A slower insertion rate would change the calibration slightly. The data were collected using the BTi SQUID susceptometer in the Physics Department at the University of Illinois. The right of the figure presents a schematic diagram of the detection region of a SQUID susceptometer. The indicated coil geometry is that of the BTi susceptometer. The sample is moved vertically through the opposing, matched detection coil pairs (Helmholtz pairs) by a stepper motor (not shown). The detection coil pairs and sample are in a stable and uniform axial magnetic field (H) produced by a persistent mode superconducting magnet (not shown) and shield (not shown). The sample is thermally isolated from the 4.2 K superconducting pickup coil system. Sample temperature is controlled by heated helium gas flowing through the sample dewar (not shown). The superconducting pickup coil system is a single closed superconducting circuit. The SQUID detector electronics are not shown. For more details see reference 10.

A stable and uniform magnetic field produced by a

[2]This is an accurate statement as far as the superconducting loop itself is concerned. However, the susceptometer's response is slowed due to the presence of normal metals in the vicinity of the superconducting loop. For the BTi SQUID susceptometer these are the metal sample dewar wall and the metal coil former. Eddy currents in these neighboring normal metals effectively slow the susceptometer's response to flux changes arising from changes in the sample's position or from magnetization changes induced (by a light pulse, for example) in a fixed sample. The response of the BTi SQUID susceptometer is further limited by a normal resistive shunt across the SQUID input introduced by the manufacturer to reduce the effects of vibration and external RF interference. These effects combine to produce a response time of ~6 ms in the BTi instrument.

persistent mode superconducting magnet is applied parallel to the axis of the detection coils. The field must be extremely stable since the pickup coil system will respond to any flux changes including those arising from the magnet.

The coil geometry of the BTi susceptometer consists of two separate, matched, opposing coil pairs (see Fig. 1). Each coil pair is designed to give a position independent response to a small sample (length <1 cm) near the coil pair's center. The BTi instrument's electronics read out two peak to peak difference signals for each round trip of the sample through the two detection coil pairs. These two readings are averaged to eliminate the effects of drift. The result is a sample magnetization measurement, which is essentially independent of sample geometry for small samples.

In a metalloprotein experiment the SQUID susceptometer measures the magnetization parallel to the applied field for a sample of randomly oriented molecules. Because the induced field of a typical metalloprotein sample is extremely small compared with the applied field, demagnetization effects can be ignored.

The thermodynamic definition of a component of the magnetization is

$$M_\alpha = N_A \frac{\sum_i (\partial E_i/\partial H_\alpha) \exp(-E_i/kT)}{\sum_i \exp(-E_i/kT)} \qquad \alpha = x, y, z,$$

where N_A is Avogadro's number, k is the Boltzmann constant, T is absolute temperature, H_α is the component of the magnetic field in the direction of M_α, and E_i are the energy levels of the paramagnetic system. In most cases the orbital moment is quenched, and M_α may be expressed in terms of the electronic spin (S) as

$$M_\alpha = N_A g_e \beta \langle S \rangle_{T\alpha},$$

where g_e is the gyromagnetic ratio of the electron, β is the Bohr magneton, and $\langle S \rangle_{T\alpha}$ is the αth component of the thermally averaged spin expectation value.

The magnetic properties of an isolated spin multiplet can often be described with the effective spin Hamiltonian

$$H = D\{[S_z^2 - S(S+1)/3] + (E/D)(S_x^2 - S_y^2)\} + \beta \mathbf{S} \cdot \mathbf{g} \cdot \mathbf{H}.$$

Here D and E/D are the zero-field splitting parameters. This quadratic spin Hamiltonian is widely used and provides a convenient means of summarizing and comparing results of EPR, electron-nuclear double resonance (ENDOR), Mössbauer, low temperature magnetic circular dichroism (MCD), and magnetization studies (11). Although it has been used successfully to describe the magnetic properties of many metalloproteins, its underlying assumption of an isolated spin multiplet must be verified in each case and may not always apply.

Comparative studies of the zero-field splitting parameters of metalloproteins with those of model compounds can give information about the ligand structure of the paramagnetic site. For proteins, a magnetization study is the method of choice for measuring D and E when the magnetic state does not yield an EPR signal. Integer spin states are usually EPR silent. In addition, relaxation broadening or severe anisotropy in the induced moment can cause half-odd integer states to be EPR silent.

The powder average magnetization is computed by calculating the projection of the magnetization of a randomly oriented molecule along the applied field direction and summing over all orientations of the molecule. A fifteen point grid for this numerical integration yields results well within 1% of the results found using any finer grid.

The curve of maximum magnetization for a specified spin (S) is found with $D = E = 0$ and is called the Brillouin curve. The magnetization for any non-zero value (positive or negative) of D will lie below the Brillouin curve when $S > \frac{1}{2}$. For $S = \frac{1}{2}$ the magnetization follows a universal curve as a function of $\beta H/kT$. For all higher spin values the zero-field splitting parameters break this universal Brillouin curve into families of curves resulting in substantial differences between data collected at fixed fields (isofield curves) and those collected at fixed temperatures (isotherms).

As an example of the effects of the zero-field splitting parameters on the magnetization, the results to be expected for the FeMo-co centers (or M centers) of the native MoFe-protein of nitrogenase are shown in Fig. 2.

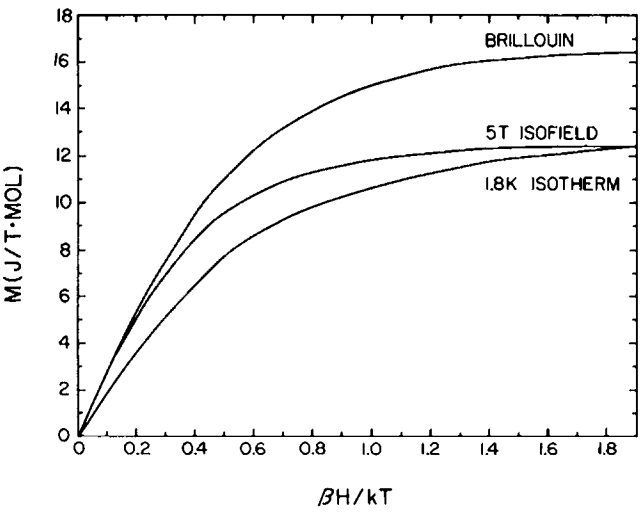

FIGURE 2 The theoretical molar magnetization for spin $S = \frac{1}{2}$ plotted against $\beta H/kT$. The Brillouin curve (maximum magnetization for spin $S = \frac{1}{2}$) was calculated assuming $D = E = 0$ in the spin Hamiltonian. The high field isofield curve was calculated with the field fixed at $H = 5$ T, using the reported zero-field splitting parameters of the FeMo-co centers of the MoFe-protein of nitrogense ($D_M = 6.1$ cm^{-1} and $E_M/D_M = 0.055$). The low temperature isotherm curve was calculated with the temperature fixed at $T = 1.8$ K using the same zero-field parameters.

These calculated curves will be used in our discussion of the native MoFe-protein of nitrogenase to be given in Section IV (see Fig. 9 *A*). EPR (12, 13), Mössbauer (14–17), and ENDOR (18) measurements have determined that the FeMo-co centers have spin $S_M = 3/2$ and zero-field splitting parameters $D_M = 6.1\ cm^{-1}$ and $E_M/D_M = 0.055$. (The subscripts refer to the *M* centers of the MoFe protein.) In Fig. 2 the magnetization in SI units per mole spin is plotted against $\beta H/kT$ out to the maximum value achieved by the BTi susceptometer. Three magnetization curves are shown: (*a*) the Brillouin curve, (*b*) the high field isofield curve, and (*c*) the low temperature isotherm curve.

The isofield curve at the susceptometer's maximum field (5 T) will always lie above the isotherm curve at the susceptometer's lowest temperature (1.8 K), as it does here. For this particular spin system all magnetization data collected at fields below 5 T and above 1.8 K will lie between these two curves, that is, within the "boomerang"-shaped region. For the case of an unknown metalloprotein state in a homogeneous sample with few impurities, the measured shape of the "boomerang" can be used to determine the concentration, spin, and zero-field splitting parameters of the unknown state.

Our goal is to measure both isofield and isotherm curves to characterize the magnetic properties of metalloproteins. Presently ferromagnetic or superparamagnetic impurities in our sample holders (discussed in the next section) make it difficult to measure isotherms. Isotherm data will also require careful matching of the sample with a diamagnetic control. In the meantime we have collected three or four isofield curves to characterize each sample.

The slope at small $\beta H/kT$ of an isofield curve (the Curie limit) can be used to measure the effective number (n_{eff}) of Bohr magnetons in the sample. Over the linear, high temperature portion of the fixed-field, molar magnetization data, the molar susceptibility ($\chi_M = M/H$) is given by

$$\chi_M = N_A \frac{n_{eff}^2 \beta^2}{3kT},$$

where $n_{eff}^2 = g^2 S(S+1)$ is the square of the effective number of Bohr magnetons. Expressing this in terms of the slope (m) of the high temperature, linear region of the isofield molar magnetization (in $J/T \cdot mol$)[3] versus $\beta H/kT$ curve we have

$$n_{eff}^2 = \frac{3}{N_A \beta}\left\{\frac{k}{\beta}\left[\frac{\Delta(M)}{\Delta(H/T)}\right]_H\right\} = 0.53716\ m.$$

[3]SI units are used throughout this paper. To convert to cgs units: $M(\text{erg/(gauss mol)}) = 10^{-3} M(\text{J/[T mol]})$, $X(\text{erg/(gauss}^2\text{ mol)}) = 10\ X(\text{J/[T}^2\text{ mol]})$.

It is often necessary to present the magnetization (M') of a single sample in units of $\mu J/T \cdot$sample (rather than per mole) since different samples in the same study may contain differing levels of impurities, thus making comparison per mole protein difficult. Or the data may be from a composite of holder and sample material (as is the case for the raw data before subtraction of the control). The relationship between the slope (m') of such single sample data and the molar magnetization slope (m) is

$$m = \frac{m'(\mu J/T \cdot \text{sample})}{cV(\mu\text{mol/sample})},$$

where cV is the product of the protein concentration c (mM) and the sample volume V (ml). If background signals are present, they must be subtracted before this conversion is made.

III. METHODS

A. General Considerations

High precision is required to detect the temperature dependent paramagnetism of a metalloprotein in the presence of the large diamagnetic contributions of the protein, solvent, and sample holder. For example, we have studied samples whose paramagnetic magnetization at 1.8 K is on the order of several percent of the sample's diamagnetism. To measure this paramagnetism to 1% requires data reliable to better than parts per thousand. This precision can be achieved with the SQUID susceptometer using the techniques we have developed.

High precision data are collected on a sample from 1.8 to 200 K at several fixed magnetic fields. Similar data are then collected on a control in a matched holder. The difference data are calibrated to ±2% by comparison with a standard platinum susceptibility sample obtained from the National Bureau of Standards. The amount of protein in the sample is determined by combining a concentration measurement (± >3%) with a precise volume measurement (±1.5%). The procedures to be detailed here focus on the temperature dependence of the difference data. These procedures are tolerant of slight changes in total sample mass during handling (caused, for example, by condensation or sublimation of water) as long as the amount of protein in the sample is unchanged. Peak to peak readings are taken upon insertion of the sample through the two opposing detection coil pairs. The problem of the potential lack of registry of the holder and sample signals (19) is eliminated by taking the difference between filled, matched buckets for sample and control.

Proper handling of a commercial SQUID susceptometer is required to obtain reproducible data at this level of precision. For example, the BTi instrument produces National Bureau of Standards traceable readings for sample magnetization (±2%), magnetic field (±0.5% for $H >$ 0.3 T), and temperature (±0.5%) in the high temperature mode (above 5 K). However, calibration of sample temper-

ature is required in the low temperature mode (to below 2 K). This calibration can be affected by superfluid film creep and by the instrument's thermal history. Moreover these effects differ from instrument to instrument. Every instrument requires thorough precooling of the sample dewar before calibration or data collection at the lowest temperatures. We calibrated the University of Illinois BTi susceptometer below 5 K using a calibrated germanium resistance thermometer. This thermometer was suspended at the center of the detection coils on a string. Four No. 42 constantan wires served as electrical leads without introducing a significant heat leak from room temperature.

With some instruments helium transfers can freeze the top plate causing air contamination of the sample dewar vacuum space. This can lead to erratic SQUID readings that are caused by very small amounts of paramagnetic oxygen condensed on surfaces in the sample dewar vacuum that are near the detection region. Gentle helium transfers and periodic bakeout of the sample dewar vacuum are required to maintain high performance. Because the sample is suspended from a flexible tape from the top of the BTi instrument four feet above the detection region, the instrument must be carefully leveled and the sample bucket suspended properly to ensure smooth vertical motion of the sample.

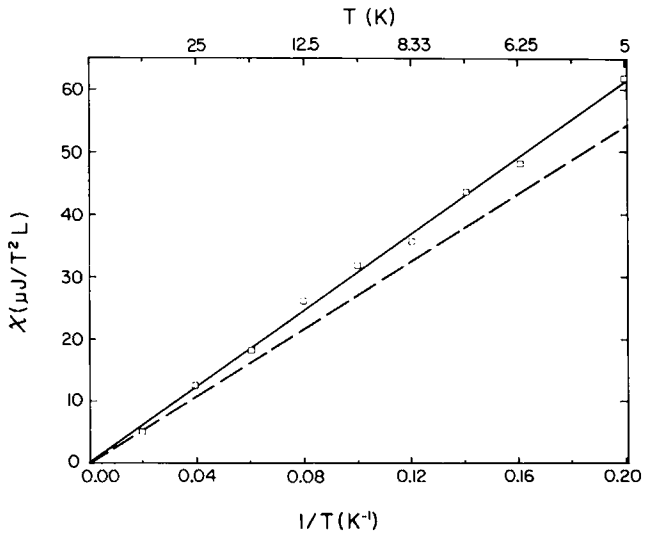

FIGURE 3 Volume susceptibility of helium gas (0.21 ml) measured at 1 T plotted in SI units against inverse temperature. The sample magnetization of an evacuated and sealed quartz bulb was first measured. The quartz bulb was then opened to the susceptometer's atmosphere of helium gas and its sample magnetization remeasured. The differences in these readings (divided by the field and by the quartz bulb's inside volume) are plotted. This set of difference readings has been translated vertically to give zero intercept. The volume of helium gas contained in the open quartz bulb was determined by weighing the bulb empty and filled with water. The solid line is a least squares fit to the nine data points. The dashed line is the calculated susceptibility of diamagnetic helium treated as an ideal gas at 1.14 atmospheres. (The static pressure above the liquid helium bath was 2 psi. Sample temperature is controlled using gas drawn from above the liquid helium bath.) The data were collected using the BTi SQUID susceptometer in the Physics Department at the University of Illinois and were presented previously (2).

B. Helium Gas Background

Helium gas flows through the detection region of the BTi SQUID susceptometer to control the sample temperature. The magnetization of this helium gas is readily detected (2) (Fig. 3) and must be considered in measuring protein samples. With the protein sample centered in the upper detection coil the signal is at its peak value. This peak signal measures the net difference between the magnetizations in each coil. This corresponds to the magnetization of the sample minus the magnetization of an equal volume of helium gas (in the opposing lower detection coil). Since helium is diamagnetic and in the opposing coil, this results in a positive, additive signal that reduces the magnitude of the negative reading for the dominantly diamagnetic sample magnetization. Furthermore, the density of the helium gas in the detection region varies inversely with temperature, producing a signal that is indistinguishable from that due to paramagnetism within the sample, as shown by our experimental results in Fig. 3. The inverse temperature dependence of the density of the displaced helium gas contributes the same slope as would a concentration of 0.18 mM of spin $S = \frac{1}{2}$ electrons. For example, at 5 K the helium gas signal decreases the measured diamagnetic magnetization of a 0.20 ml buffer sample by several hundred times the noise level of the instrument (several percent of the sample's diamagnetism). This effect is eliminated by collecting data on a carefully matched sample volume and subtracting (see Fig. 7, *A* and *C*).

C. Oxygen

The signal of the spin $S = 1$ paramagnetism of molecular oxygen in air-saturated buffer (oxygen concentration of 0.25 mM) frozen from 30°C is equivalent in the Curie region to that contributed by a concentration of 0.67 mM spin $S = \frac{1}{2}$ electrons. Moreover this signal shows saturation behavior similar to that of the metalloproteins we are studying. When saturated at high fields (5 T) and low temperature (1.8 K) the signal due to molecular oxygen is several hundred times the noise level of the susceptometer. Thus both in form and magnitude the oxygen signal is comparable to the signals under study. Our general approach to this problem is to exclude molecular oxygen from both the sample and its matched control.

Oxygen is rigorously excluded from the sample during the strictly anaerobic preparation of oxygen-sensitive metalloproteins such as nitrogenase. The matched controls for these experiments are loaded and frozen in the same manner using an anaerobic glove box or anaerobic glassware. At the other extreme are cases where molecular oxygen introduced through air saturation of the sample is used to produce the fully oxidized protein. In such cases we remove the oxygen, after protein oxidation, either physi-

cally or enzymatically. Physical removal can be accomplished, for example, by gentle stirring of the sample under a gentle flow of humidified argon for 45 min (20) or by subjecting the sample to one or more freeze-pump-thaw cycles. Enzymatic removal can be accomplished by adding catalytic amounts of a dioxygenase with excess substrate and stirring before freezing (21).

Molecular oxygen in air may condense onto the outer surfaces of the frozen samples during loading into the susceptometer. This is routinely "baked off" by holding the sample above 100 K for several minutes within the flowing helium gas of the susceptometer. Two checks can be made to verify that the oxygen has been completely removed. Large amounts of oxygen frozen onto the sample holder's outer surface cause a significant distortion in the shape of the insertion signal observed as the sample is moved between the two opposing detection coils. (See Fig. 1 for an example of an undistorted signal.) Monitoring the shape of the insertion signal before and after warming the sample to 100 K serves as one check on the presence of oxygen. If the magnetization of the sample is then studied from 5 K to well above 40 K, residual oxygen contamination will be detected as a peak near 40 K at the antiferromagnetic transition (the Néel point) of solid oxygen. Warming for longer periods above 100 K will remove this residual oxygen. Experience in recognizing and eliminating these signatures of oxygen contamination will dictate the bakeout sequence required for a particular sample and holder configuration.

We now have extensive data on empty holders and controls and know the signature of the impurities typical of each type of sample holder. (See Fig. 5 for a typical control in a quartz bucket and Fig. 7 *B* for a typical control in a boron nitride bucket.) This information is used in each metalloprotein study to verify that the control is not contaminated with unexpected paramagnetism, such as oxygen. This in turn serves as a check on the sample, as long as the sample and control were prepared and handled similarly.

All of the magnetization data presented in this report were collected soon (within days) after loading sample holders with sample. Recently we have seen spurious results for samples reexamined after being stored for several months under liquid nitrogen. The difficulty appears to be due to oxygen accumulation during storage.

D. Spin ½ Nuclei

We began these studies knowing that the nuclear spin magnetization of the protons in water is readily detected by the SQUID susceptometer (1). Protons in water have a concentration of 110 M. The square of the ratio of the proton moment to the electron moment is $(\mu_p/\mu_e)^2 = (1/660)^2 = 2.3 \cdot 10^{-6}$. Therefore the proton nuclear spin susceptibility contributes the same Curie law slope as a concentration of 0.25 mM spin ½ electrons.

We expected to be able to subtract the nuclear paramagnetism of the protons of water using a matched control much as we have subtracted the helium gas background. However, at low temperatures the nuclear paramagnetism of the protons is difficult to subtract because it has relaxation times on the order of several hours (see Fig. 4 *A*) (3). Moreover its relaxation rate changes dramatically in the presence of the electronic paramagnetism under study. That is, the electronic spins act to relax the protons. Proton relaxation in these frozen samples is governed by the presence of fixed sites of electronic paramagnetism, either

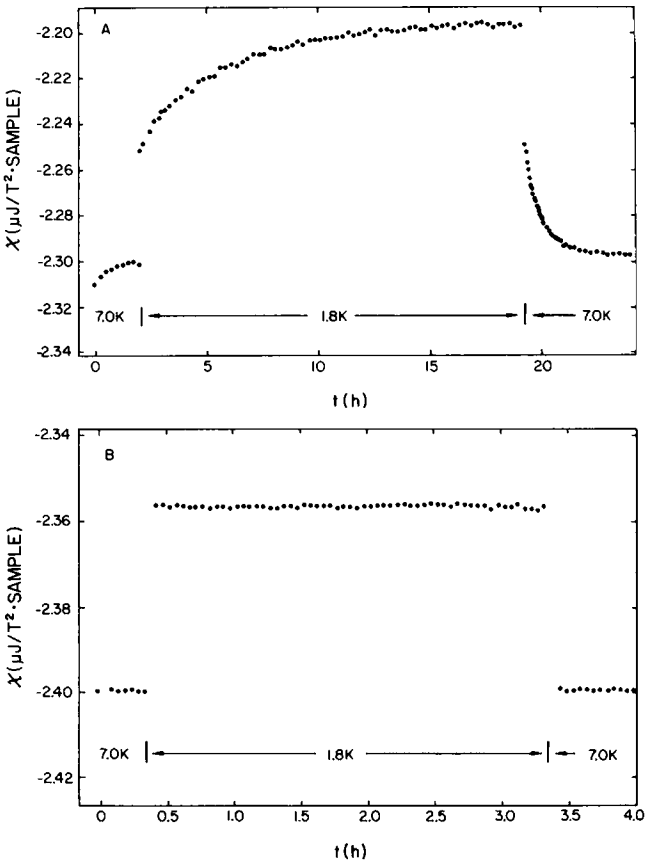

FIGURE 4 Relaxation kinetics of (*A*) protons and (*B*) deuterons. The sample susceptibility is plotted in SI units against time. The vertical axis indicates the sample's net diamagnetism as negative numbers increasing in magnitude vertically downward. The magnetic field was 0.8 T. Each point represents the average of data collected during 15 round trips of the sample between the instrument's detection coils. This takes ~3 min. The data were collected using the BTi SQUID susceptometer in the Physics Department at the University of Illinois. (*A*) Relaxation kinetics of the proton nuclear susceptibility of an H_2O sample (0.18 ml) in a quartz holder (0.30 g). The time interval from completion of one point to the completion of the next point is ~15 min. The sample was initially at 7.0 K. The sample temperature was changed to 1.8 K at time t = 2.0 h and back again to 7.0 K at time t = 19.2 h. (*B*) Relaxation kinetics of the deuteron nuclear susceptibility of a D_2O sample (0.18 ml) in a quartz holder (0.32 g). The time interval from completion of one point to completion of the next point is ~ 3 min. The fully equilibrated sample as initially at 7.0 K. The sample's temperature was changed to 1.8 K at time t = 20 min and back to 7.0 K at time t = 3 h 20 min. Each sample contained an unknown amount of fast relaxing electronic paramagnetism.

impurities or metalloprotein centers. Protons close to these sites relax rapidly. Protons far from these sites relax much more slowly through the process of nuclear spin diffusion to the fixed sites of electronic paramagnetism. The net effect is that the magnitude of the slow component of the nuclear magnetization changes from sample to control. Therefore subtraction of the unwanted nuclear signal is not straightforward. We were the first to notice this source of irreproducibility in susceptibility studies (2). It very probably was the noise source limiting previous metalloprotein studies, which had a noise level corresponding to a concentration of ~ ±0.2 mM spin ½ electrons (20, 22, 23).

That the magnitude of the slowly relaxing component of the proton's nuclear magnetization varies from sample to control makes physical techniques for dealing with this problem impractical. For example, radio frequency saturation could be used to drive the nuclear magnetization to zero immediately before each magnetization measurement. However, before completion of the magnetization measurement the fast relaxing components of the proton magnetization would be affecting the data. Since the fraction of the proton population that relaxes rapidly varies from sample to control the difference data would include an unknown contribution from the proton magnetization. Similar problems occur using the technique of raising the sample from the detection region towards the instrument's airlock. This would place the sample in a low magnetic field (effectively zero relative to the detection region) and raise its temperature until the proton relaxation is rapid. However by the time the next magnetization datum was collected the fast relaxing components of the proton magnetization would be affecting the data. Only by maintaining radio frequency saturation during the magnetization measurement will it be possible to remove the spin $I = ½$ nuclear noise source using physical techniques.

Use of a deuterated buffer eliminates this noise source. The magnetic moment of the deuteron is smaller than that of the proton. The square of the ratio of the deuteron moment to the proton moment is $(0.857/2.793)^2 = 0.094$. Therefore for a fully deuterated sample, the deuteron nuclear susceptibility contributes the same Curie law slope as a concentration of 24 μM spin ½ electrons (see Fig. 7 *B*). More significantly, the deuteron has an electric quadrupole moment, which results in rapid relaxation. Since the nuclear paramagnetism of the deuteron equilibrates quickly (see Fig. 4 *B*), it is properly measured immediately in both sample and control and, therefore can be easily subtracted. With the present sensitivity of the SQUID susceptometer, 99% deuteration of the magnetization sample is adequate to eliminate the slowly relaxing proton signal as a noise source. The signal of nonexchangeable protein protons is usually too small to detect.

At 1.8 K a commercial SQUID susceptometer can detect any nuclei having a signal comparable to that of protons at a concentration of 500 mM. For this reason all spin $I = ½$ nuclei (H, F, . . .) must be kept to a minimum if their slow and varied relaxation rates are to be insignificant in magnetization studies of metalloproteins. For example, most plastics (such as Teflon with the spin $I = ½$ fluorine, or delrin with the spin $I = ½$ proton) must be avoided. We now use sample holders made of quartz or boron nitride. Neither of these materials contain detectable levels of spin $I = ½$ nuclei.

E. Sample Holders

An uncapped holder works well for studies below 200 K even when used with samples that must be kept strictly anaerobic. Sample holder buckets are made by the University of Minnesota glassblower in batches of 20 from 8-mm OD Supersil (Heracus Amersil, Sayreville, NJ) quartz tubing. A pair of small holes for the suspension thread is drilled near the top of each bucket with a diamond drill. The buckets are then weighed and paired by mass after having been etched overnight in 10% hydrofluoric acid.

Equal volumes of sample and its control are separately loaded into the uncapped cups using a gas-tight, calibrated syringe (Hamilton Co., Reno, NV). Calibration of the syringe is accomplished by weighing a volume of water (measured by ejection from the syringe) using an analytical balance. The sample and control are frozen while still in an anaerobic atmosphere and stored under liquid nitrogen.

Loading of the frozen sample into the susceptometer is accomplished by hooking the sample holder suspension thread onto the instrument's suspension bobbin while keeping the sample under liquid nitrogen in a hand dewar. The dewar is then removed and the airlock lid placed over the sample. The airlock is then rapidly purged of air and backfilled once or twice with helium gas. Finally the sample, while still frozen, is lowered into the cold instrument. The total time from removal from liquid nitrogen gen until insertion into the susceptometer is less than 2 min. Removal of the frozen sample from the cold instrument to liquid nitrogen is accomplished in a similar fashion. It is important to have the instrument sample temperature set cold (well below liquid nitrogen temperature) both during loading and unloading to avoid thawing the sample during the relatively slow insertion and removal process. If static charge on the sample is a problem it can be neutralized by spraying with positive and negative ions using a piezoelectric gun (20).

Above 200 K loss of sample through sublimation will render an uncapped holder useless (20). For these experiments we have used spherical quartz bulbs (≈6-mm OD) (sketched in Fig. 1) sealed by a silicone plug. To guarantee a tight seal at cryogenic temperatures, the clear silicone was stretched lengthwise, frozen in liquid nitrogen, and inserted while frozen into the neck of the bulb and then cut to size. After thawing, the plug forms an extremely tight seal. A single strand of nylon thread through the silicone plug and knotted at the end inside the bulb serves to

suspend the sealed holder. This holder can be purged of air, loaded with an anaerobic protein sample, and later injected with CO, if desired, using syringes and an appropriate gas handling manifold. This seal worked well above 2.2 K. However, immersion into superfluid helium led to spurious magnetization readings since superfluid leaked into the holder. One such sealed sample holder exploded on warming.

In our studies of iron containing metalloproteins we routinely collect Mössbauer data on our ^{57}Fe-enriched magnetization samples. This is done to characterize our sample directly. Quartz is quite opaque to the gamma rays of Mössbauer spectroscopy and is impractical as a sample holder material in such studies. We use boron nitride instead.

Our present boron nitride holders are uncapped cups with 6.8-mm OD, 9.0-mm length, and 0.5-mm wall thickness. The pyrolytic boron nitride cups are manufactured by Union Carbide Corp. (Cleveland, OH) using a vapor deposition process. These are etched overnight in 10% hydrofluoric acid and weighed. Buckets having similar masses are paired for use as holders for sample and control. The loop of suspension thread passes through two small holes on opposite sides near the top of the sample cup. A fine coating of silicone grease over the lower ends of the thread prevents sample material from moving up the thread by capillary action. Sample volume is ~0.18 ml. Larger diameter holders (up to 7.4 mm) were tried and found to give spurious results. The present diameter (6.8 mm) matches that of the largest sample holder supplied by the manufacturer of the SQUID susceptometer. Our quartz sample holders have similar outer dimensions but thicker walls yielding a sample volume of ~0.15 ml.

F. Ferromagnetic and Superparamagnetic Impurities

Ferromagnetic impurities commonly present in sample holder materials are readily detected by the SQUID susceptometer. For example, Cabrera (24) used a SQUID magnetometer in zero applied field to study the remanent magnetizations of over 50 materials. He found that plastics (delrin, nylon, Teflon, polyethylene) contain detectable ferromagnetic impurities even after careful cleaning of their surfaces with acid. On the other hand, the remanent magnetizations of quartz and of aluminum were too small to be detected once these materials had been carefully cleaned to remove surface contamination. We now routinely etch our quartz holders with hydrofluoric acid to remove surface ferromagnetic impurities. Superparamagnetic impurities remain (see Fig. 6).

Superparamagnetism results when small, single domain ferromagnetic particles are present. At higher temperatures (above the blocking temperature [T_B]) thermal agitation is adequate to produce zero remanence and no hysteresis (25). Below the blocking temperature, superparamagnetic impurities show all the characteristics of ferromagnetic impurities.

Our goal is to eliminate ferromagnetic impurities from our sample holders. In the meantime, we collect and analyze our data so as to minimize the effects of the ferromagnetism on our data. We have not thoroughly studied the ferromagnetism itself. This will be done eventually if it proves impossible to eliminate it.

Hysteresis due to ferromagnetic impurities can be avoided by working at magnetic fields that are large enough to saturate the ferromagnetism. We routinely work at fields >0.3 T for this reason.

Even at fields large enough to saturate the ferromagnetic impurities, the impurities affect the magnetization data in two ways. At a fixed high field (above 0.3 T) the temperature dependence of these impurities becomes readily detectable at high temperatures (above 70 K) (see Fig. 5). This can limit metalloprotein magnetization studies to temperatures below 70 K. Impurities also cause a significant field dependence in the intercept (B_H) of a plot of susceptibility versus inverse temperature (see Fig. 6). This field dependence makes the direct measurement of a magnetization isotherm difficult.

In Fig. 5 the sample susceptibility of D_2O in an etched

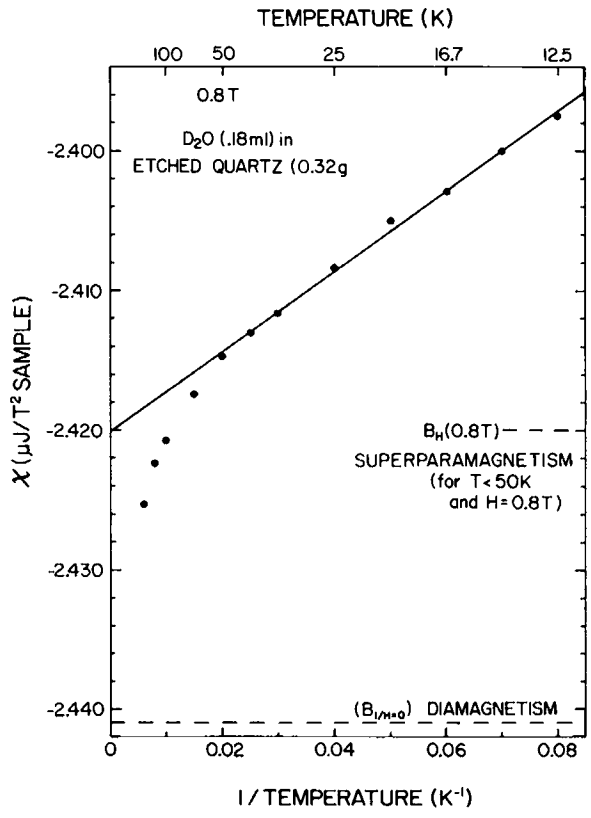

FIGURE 5 The sample susceptibility of D_2O (0.18 ml) in an acid-etched quartz cup (0.32 g) plotted in SI units against inverse temperature. The field was 0.8 T. Each point represents the average of data collected during 15 round trips of the sample between the SQUID susceptometer's detection coils. The data were collected using the BTi SQUID susceptometer in the Physics Department at the University of Illinois.

quartz holder is plotted against inverse temperature. This sample is expected to be diamagnetic, showing no temperature dependence (apart from the very small remaining nuclear paramagnetism of the deuterons). Indeed its susceptibility would appear temperature independent (within noise of horizontal) if measured by an instrument lacking the sensitivity of a SQUID susceptometer. The slope of the solid line in Fig. 5 contains contributions from the density changes of the displaced helium gas (~30% of the total slope) (see Fig. 3), from impurity electronic paramagnetism in the D_2O and quartz (~60% of the total slope), and from the nuclear paramagnetism of the deuterons (<10% of the total slope) (see Fig. 7 *B*). The deviations at high temperatures (above T_B) from this linear behavior are due to superparamagnetic impurities in the etched quartz.

The intercept (B_H) of the solid line of Fig. 5 depends on the field when superparamagnetic impurities are present. This is shown in Fig. 6. For example, the four points

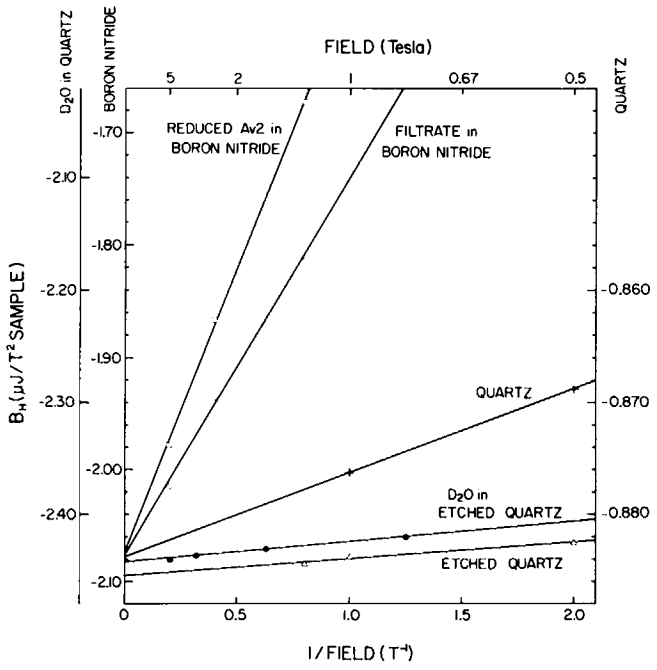

FIGURE 6 The Curie law intercepts (B_H) of sample susceptibility at several fixed fields plotted in SI units against inverse field for five samples. For the D_2O sample (0.18 ml) in acid etched quartz (0.32 g) (*solid circles*) the net diamagnetic susceptibility is shown on the outer left vertical scale. For the samples (0.18 ml) in the boron nitride holders (0.199 g) (*open symbols*) the net diamagnetic susceptibility is shown on the inner left vertical scale. The net diamagnetic susceptibility of the empty quartz holders (with acid etching [0.226 g] [*open triangles*]; without acid etching [0.225 g] [*crosses*]) is shown on the right vertical scale. These three vertical scales are identical but have been translated vertically relative to one another for clarity of presentation of the three sets of data. The Curie law intercept at each field (B_H) was found by plotting the sample susceptibility at that fixed field against inverse temperature and fitting the appropriate range of high temperature data to a straight line (see Fig. 5). The slopes in the present figure are a measure of the ferromagnetic or superparamagnetic impurities of each sample and holder. The intercepts ($B_{1/H\to 0}$) are a measure of the diamagnetism of each sample and holder.

labeled D_2O in etched quartz in Fig. 6 were derived from temperature dependence studies of this sample and holder at fields of 5, 3.2, 1.6, and 0.8 T. (The 0.8 T data are shown in Fig. 5.) The slope of the line through these points in Fig. 6 is a measure of the superparamagnetic impurities in the etched quartz holder and the D_2O sample. (The line for a separate study of etched quartz indicates the impurities in the holder alone.) The intercept ($B_{1/H\to 0}$) of this inverse field plot measures the diamagnetism of the sample and its holder. This inverse field intercept ($B_{1/H\to 0}$) found in Fig. 6 for D_2O in etched quartz has been indicated as a horizontal dashed line labeled diamagnetism in Fig. 5. For this sample and holder, the contribution from superparamagnetic impurities at 0.8 T is comparable to that of the paramagnetic impurities and background helium at 12 K. These two contributions (offset of intercept and slope) are each slightly <1% of the diamagnetism.

The boron nitride sample holders used in our combined Mössbauer and SQUID magnetization study of the reduced Fe-protein of nitrogenase (see next section and Figs. 7 and 8) contain ferromagnetic impurities, as can be seen from Fig. 6. These holders were machined from a rod of boron nitride (Grade HBR) supplied by Union Carbide Corp. We no longer use this material for sample holders because it contains too much ferromagnetism; pyrolytic boron nitride is used instead. These impurities contribute about 20 times the field dependence as do the superparamagnetic impurities of the sample of D_2O in etched quartz. The mismatch in the ferromagnetic impurities of the two boron nitride holders, as indicated by the different slopes in Fig. 6, results in the relatively large offset (seen in Fig. 7 *A*) in the raw data at a fixed field of the sample compared with the control.

The sample and control of the reduced Fe-protein in boron nitride holders are matched in their net diamagnetism as their inverse field intercepts ($B_{1/H\to 0}$) shown in Fig. 6 indicate. This match in diamagnetism occurred despite the fact the sample contains protein and the control does not. (The apo-protein would be expected to change the signal by only six parts in ten thousand. This is near the noise level of the instrument.) At these signal levels, ferromagnetic impurities in sample holders are likely to cause an offset in the difference data even when great effort is made to match the diamagnetism of sample and control.

When the sample and control each contain significant ferromagnetic impurities, it is important to collect data at each field without removing the sample from the field and without resetting the magnet. Such interruptions in the collection of isofield data can cause offsets within the data set due to changes in the remanent magnetization of the ferromagnetic impurities of the sample holder.

G. Automatic Data Collection

Computer software to automate data collection from the BTi susceptometer was developed at the University of

Illinois during these studies.[4] This software enables convenient use of an unmodified BTi instrument. The program first determines that thermal equilibrium has been reached after the setting of a new temperature. Sample magnetization is next recorded automatically until it has equilibrated. Several different threshold criteria can be set to determine when equilibration of sample magnetization has occurred. This use of the sample magnetization as a criterion for equilibration is a unique feature of the Illinois software (26). A specified number of points is then recorded and averaged. Extreme outliers are rejected during this process. The process is repeated automatically at specified temperatures either over the high temperature range (above 5 K) or over the low temperature range (to below 2 K). The program can be set to record data properly even when the magnetization takes a long time to equilibrate, as when protons are present. In addition, the temperature can be made to approach the next setting without overshooting.

IV. MAGNETIZATION OF THE NITROGENASE PROTEINS

We are currently applying these magnetization techniques to a variety of metalloproteins. As examples, we will discuss our results on the Fe-protein (7) as well as unreported results on the MoFe-protein of nitrogenase from *Azotobacter vinelandii*. The physical biochemistry of both proteins has been reviewed recently (27, 28).

In the case of the published Fe-protein study we want to present the (previously unpublished) raw magnetization data and the full details of the data reduction process as an example of procedures we are using in many of our current metalloprotein studies.

A. Fe-Protein

In a recent EPR, Mössbauer, and magnetization study of the Fe-protein (7), we found that the protein's [4Fe-4S]$^{1+}$ cluster has a solvent-dependent spin state. In aqueous buffer, ~40% of the molecules contain clusters with spin $S = \frac{1}{2}$ ground states, while the remainder have clusters with spin $S = \frac{3}{2}$. The former state yields the $g = 1.94$ EPR signal typical of [4Fe-4S]$^{1+}$ clusters, whereas the latter exhibits signals at $g = 5.8$ and 5.1, indicative of the newly discovered $S = \frac{3}{2}$ spin state.

Sample Characterization. The Fe-protein was purified and characterized as described in reference 7. The concentration of cluster (0.32(2) mM) was estimated to be 25% of the iron concentration. The protein concentration (0.37 mM, assuming $M = 63{,}183$ [29]) and purity (~85%) were consistent with this estimate. The sample was equilibrated in buffer containing D_2O (50 mM Tris, pD 7.5, 2 mM sodium dithionite), loaded into a boron nitride holder using a calibrated Hamilton Co. syringe, and frozen anaerobically. A control, consisting of an equal volume of the filtrate from the final concentration step in the preparation of the protein, was similarly prepared.

The ^{57}Fe-enriched sample was studied with Mössbauer spectroscopy to characterize the redox state of the sample and to measure impurity levels. Analysis of the low temperature Mössbauer spectra showed that ~5% of the clusters were in the diamagnetic, oxidized state with the remainder of the clusters in the native half-odd-integer paramagnetic states. Analysis of the high temperature Mössbauer spectra indicated that 1.8(2)% of the total iron was spin $S = 2$ ferrous impurity.

EPR spectra were collected on a separate sample drawn from the same preparation. In addition to the signals characteristic of reduced Fe-protein, the spectra exhibited a weak signal at $g = 4.3$, indicative of high spin ($S = \frac{5}{2}$) ferric iron. To estimate the spin concentration of this signal we measured the Curie susceptibility of a sample of the diamagnetic, oxidized Fe-protein, which showed a similar weak $g = 4.3$ signal. Analysis indicated that ~ 4% of the spins (i.e., 1% of the total Fe) of the reduced sample were in this spin $S = \frac{5}{2}$ state.

Magnetization Data. The raw data from the magnetization study of Fe-protein in a field of 5 T are shown in Fig. 7 *A*. The SQUID magnetization readings for this sample and its control are plotted in SI units against $\beta H/kT$. Note that the saturation magnetization of the metalloprotein is <8% of the diamagnetism of the sample and holder.

Fig. 7 *B* presents the same data for the filtrate control on an expanded vertical scale. The change in slope and the offset in going from the open circles (high temperature, low $\beta H/kT$) to the closed circles (low temperature, high $\beta H/kT$) is due to the helium gas which is present at temperatures greater than 5 K (at approximately one atmosphere pressure) but absent at lower temperatures (well below 0.001 atmosphere pressure). The magnitude of this effect is proportional to the sample volume. With sample and control carefully matched in volume these effects of the helium background are canceled in the difference data as shown in Fig. 7 *C*. There is no vertical gap in the data where the open and closed symbols overlap (from 0.35 to 0.65 $\beta H/kT$).

The control data shown in Fig. 7 *B* have three more features worth noting. First, the low temperature (closed circles, high $\beta H/kT$) data have a slope due to the nuclear susceptibility of the deuterons present in the buffer. A concentration of 24 μM spin $S = \frac{1}{2}$ electrons would contribute the same slope in the Curie law region (at higher temperatures). The ability to measure this small nuclear susceptibility indicates the sensitivity of the SQUID susceptometer and the precision of the data.

[4] This software is available from Dr. Michael Weissman, Physics Department, University of Illinois at Urbana-Champaign, 1110 W. Green Street, Urbana, IL 61801.

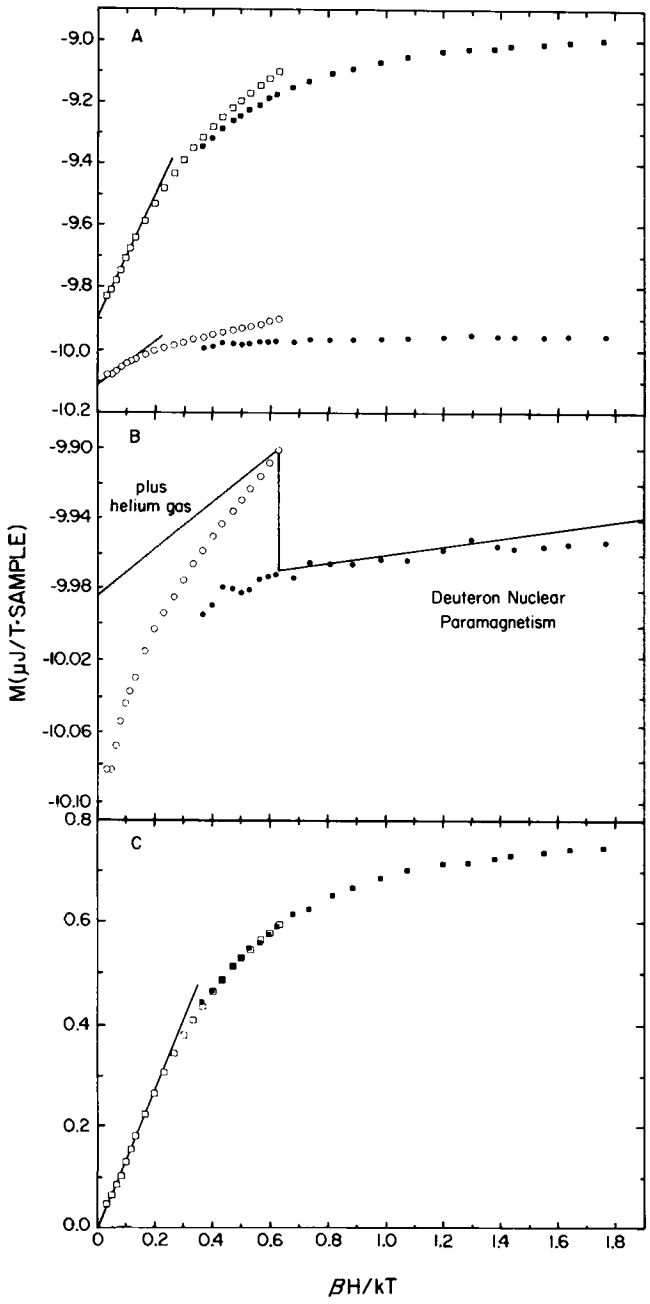

FIGURE 7 (*A*) Raw data for the sample magnetization at 5 T of the reduced Fe-protein from *A. vinelandii*. *Squares*, 180(3) μl of ^{57}Fe-enriched Fe-protein, 323(7) μM, in deuterated buffer in a 199 mg boron nitride holder. *Circles*, 180(3) μl of the filtrate (from the final concentration step) in a matched 199 mg boron nitride holder. Each point represents the average of data collected during 15 round trips of the sample between the susceptometer's detection coils. Helium gas was present at temperatures above 5 K (*open symbols*) but absent at low temperatures (*solid symbols*). The solid lines are least squares fits to the appropriate range of high temperature data for the sample and control. It is the intercepts of these lines (divided by 5 T to yield the sample susceptibility intercept [B_H]) that are plotted (at $1/H = 0.2\ T^{-1}$) in Fig. 6 for the two boron nitride holders. The data were collected using the BTi SQUID susceptometer at the National Magnet Laboratory of M.I.T. (*B*) Magnetization data for the control shown in Fig. 7 *A* plotted on an expanded vertical scale. The solid line labeled "Deuteron Nuclear Paramagnetism" was calculated assuming a volume of 180 μl D_2O. The solid line labeled "plus Helium Gas" includes contributions from both the diamagnetic helium gas within the detection region and the deuteron nuclear paramagnetism of the D_2O sample. (*C*) Difference data at 5 T for the reduced Fe-protein derived from the raw data shown in Fig. 7 *A*. The data have been translated vertically to bring the intercept to zero. The solid line is a least squares fit to the appropriate high temperature points.

Second, the worst case scatter in the data is approximately nine parts in ten thousand. The overall noise level is substantially less than this. Third, the high temperature (open circles, low $\beta H/kT$) data do not follow the linear (against inverse temperature) behavior expected from the helium gas density changes. The curvature is due to the saturation behavior of impurity electronic paramagnetism in either the filtrate or holder.

The difference data obtained by subtracting the control data from the sample data are shown in Fig. 7 *C*. The Curie region of the difference data set has been used to measure the magnetization intercept. The data set has then been translated vertically to bring the intercept to zero. It is this vertical translation of the difference data set that eliminates any mismatch (*a*) in the ferromagnetic impurities or (*b*) in the diamagnetism of the sample and control. The resulting translated difference data set is the signal due to the paramagnetism of the metalloprotein and its impurities. It is this data set that is shown as the 5 T data (closed circles) for reduced Fe-protein in Fig. 8.

Fig. 8 shows the vertically translated difference magnetization data at 5 T (closed circles) as well as similar data at fields of 2.5 T (open circles) and at 1.25 T (crosses). All of the data shown in Fig. 8 were collected on one sample and its control over a period of a week with one loading of each into the SQUID susceptometer. The actual data logging time was ~90 h. The difference magnetization data at each of the three separate fields have been translated vertically to bring each of the three intercepts to zero.

The inset of Fig. 8 contains all of the high temperature data for the reduced Fe-protein plotted as sample susceptibility in SI units against inverse temperature. The least squares fit to the linear region of the data for each field is shown in the inset and tabulated in the figure caption.

The data of Fig. 8 are the same data as published in Fig. 10 of reference 7 where our interpretation, outlined above, is described in detail.

B. MoFe-Protein

As a second example, we report a magnetization study of the MoFe protein of the nitrogenase system from *Azotobacter vinelandii*. This protein has been studied extensively with a variety of physical techniques, including room temperature susceptibility using nuclear magnetic resonance (30); for reviews see references 27 and 28. The most comprehensive information has come from a series of Mössbauer studies (14–17) which has led to the following picture. The MoFe-protein contains 30 ± 2 Fe and 2 Mo atoms. The iron atoms are organized essentially into two

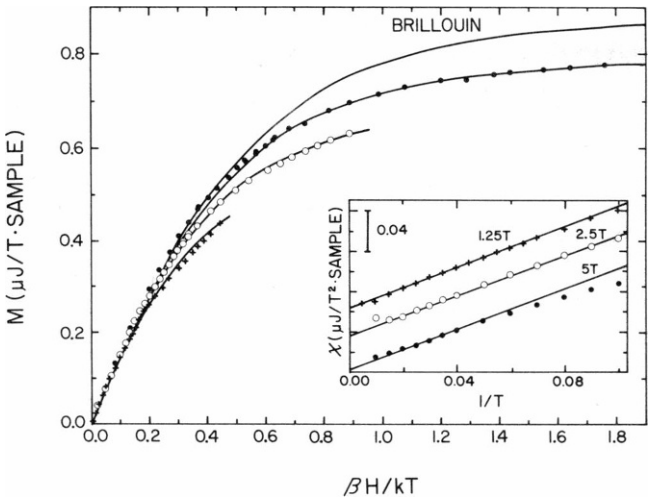

FIGURE 8 Magnetization of reduced Fe-protein from *A. vinelandii* at three fixed fields (●, 5 T; ○, 2.5 T; +, 1.25 T) plotted in SI units against $\beta H/kT$. The set of difference data (between data for the sample and its control) at each field has been separately translated vertically to bring its intercept to zero. The three solid lines through the data are calculated magnetization curves obtained by summing contributions from iron impurities (Fe^{2+}, 2% of total Fe; Fe^{3+}, 1% of total Fe) and the ground states (S_C = ½, 32% of clusters; S_C = ³/₂, 63% of clusters) of the two $[4Fe\text{-}4S]^{1+}$ cluster types as described in reference 7. (The subscripts designate the [4Fe-4S] clusters.) The solid line labeled Brillouin was obtained by summing the same contributions with the 63% spin S_C = ³/₂ cluster contribution calculated with $D_C = E_C = 0$ instead of $D_C = -3$ cm^{-1} and $E_C/D_C = 0.22$. For clarity several of the high temperature points have been omitted from the figure. (*Inset*) The high temperature difference data for the reduced Fe-protein are plotted as sample susceptibility in SI units versus inverse temperature. The symbols distinguishing data at different fields have the same meaning as in the main figure. The vertical scale of the inset is relative since the data at different fields have been offset for clarity. The range of temperatures has been chosen to include the onset of saturation at each field. The solid lines are least squares fits to the linear region of the data at each field. Several of the high temperature points have been omitted from the fits as have points judged to lie in the saturation region. The omitted high temperature points were affected by ferromagnetic impurities in the boron nitride holders. The results of these fits are tabulated below:

Field	Points included (from left)	Slope
T		*μJ/T sample*
5.000	4–7	1.56
2.500	2–10	1.50
1.250	4–16	1.48

The uncertainty in the slope found by averaging the values measured at each of the three fields is ±2.8%

types of clusters, referred to as the P-clusters (15) and the M-centers (14). The latter can be extruded from the protein (31), and are generally referred to as the molybdenum and iron containing cofactor, FeMo-co. The MoFe protein contains two FeMo-co clusters, each containing 6, or perhaps 7, Fe sites and 1 Mo. In the presence of a reductant such as dithionite the FeMo-co centers appear as a spin-coupled cluster with cluster spin S = ³/₂. The electronic properties of the S = ³/₂ system can be described by the spin Hamiltonian

$$H = D_M[S_z^2 - 15/12 + (E_M/D_M)(S_x^2 - S_y^2)] + g_o\beta \mathbf{S} \cdot \mathbf{H}.$$

From an analysis of the FeMo-co EPR signal, Münck et al. (14) determined $E_M/D_M = 0.055$ with $g_o = 2.00$. Venters et al. (18) determined $D_M = 6.1 \pm 0.1$ cm^{-1} from high-precision ENDOR data. With this information the saturation magnetization curves of the FeMo-co centers are completely specified. The remainder of the iron belongs to four P-clusters. These novel structures appear to be of the [4Fe-4S] type. In the presence of dithionite the P-clusters are in the native state, denoted P^N, which has been shown by Mössbauer to be diamagnetic ($S = 0$).

The Mössbauer data have also revealed a spectral component labeled S, representing approximately two Fe atoms in an integer spin state. (The spectral feature is a quadrupole doublet.) Presently, it is not clear whether S belongs to a separate cluster or whether it is simply a subsite in two of the P-clusters. (The Mössbauer studies have shown that the four P-clusters occur as two slightly distinct pairs.) If S is a subsite of a P-cluster, only the FeMo-co centers contribute to the paramagnetic susceptibility. If S is shown, however, to be paramagnetic, it must represent a distinct structure.

The purpose of this magnetization study of the MoFe-protein is to determine the spin of the S site.

Sample Characterization. The ^{57}Fe-enriched MoFe-protein was purified and characterized using techniques similar to those described for the Fe-protein (7). The specific activity after crystallization was 2,080 nmol C_2H_2/min per mg. The purity of the protein was over 90% according to SDS-polyacrylamide gel electrophoresis. Two samples were prepared at different times from a single preparation. After exchanging the samples into deuterated buffer, equal volumes of Sample I and its filtrate control were loaded into matched boron nitride cups using a calibrated Hamilton syringe. Sample II and its control were similarly loaded into matched etched quartz holders. A separate sample in a boron nitride cup was prepared for Mössbauer characterization of Sample II.

Characterizing these samples entails measuring (*a*) the concentration of paramagnetic impurities, (*b*) the ratio of P-clusters/M-centers/S-site, (*c*) the oxidation states of the clusters, and (*d*) the concentration of the holo-protein.

The most prevalent paramagnetic impurity was high spin ferrous iron. High temperature Mössbauer spectra indicated each sample contained 1.0(2)% spin $S = 2$ Fe^{2+} impurity. EPR spectra gave no evidence of Fe^{3+} impurity although these measurements were made difficult by the large FeMo-co signal throughout the $g = 4.3$ region. Metals besides iron could, of course, contribute to the paramagnetism of the sample. Manganese, copper, nickel, and chromium concentrations were determined by plasma

emission spectroscopy. Only copper was present at detectable levels and only in Sample II (≈0.6 equivalents); it should, however, be in the diamagnetic cuprous state in the presence of dithionite.

The P-clusters/M-centers/S-site ratios were estimated by Mössbauer spectroscopy. Both samples had essentially the same ratio of Fe in the various clusters (53% Fe belonging to the P-clusters, 40% to the M-centers, 7% to the S-site) as have all the other MoFe-protein samples that we have studied over a 10-yr period.

Oxidized and reduced MoFe-protein clusters have quite different Mössbauer spectra (14–17) and are thus readily distinguished. The Mössbauer spectra showed that both samples were completely in the dithionite-reduced, native state.

The holo-protein concentrations for both samples were determined by measuring the iron and molybdenum concentrations to avoid errors arising from the presence of apo-protein. Iron concentrations (Table II) were determined colorimetrically (32) and by atomic absorption (7) and plasma emission (33) spectroscopies. Molybdenum concentrations were determined using the latter two techniques. The holo-protein concentration of each sample was found by averaging the Fe concentrations divided by thirty and the Mo concentrations divided by two. Our estimated uncertainty in the metal determinations is ~ ±10%.[5]

Magnetization Data. To determine the spin of the S site we will first examine the Curie region of both MoFe-protein samples (I and II) using the measured protein concentrations to determine the magnetic moment of each sample (Table II). The square of the magnetic moment (n^2_{eff}) for the native MoFe-protein is found by subtracting the Fe^{2+} impurity contribution from the total. The observed average of the two samples (n^2_{eff} = 24(4)) is, within uncertainties, the value expected for native MoFe-protein containing a diamagnetic S site (n^2_{eff} = 30 for the two S = ½ FeMo-co centers). The expected value for n^2_{eff} of native MoFe-protein would be 38 were a spin S = 1 state of one S-site present in addition to the two spin S = ½ FeMo-co centers. This is ruled out by the data as are all higher integer spin states.

As seen in Table II the result for Sample I (27(4)) but not Sample II (22(2)) lies within the estimated uncertainty of the expected result (n^2_{eff} = 30). The higher protein concentration of Sample I has undoubtedly improved the reliability of each component of the measurement: (*a*) the Mössbauer spectra (the Fe^{2+} impurity level), (*b*) the Curie slope (total sample magnetic moment), and (*c*) the metal concentrations (MoFe-protein concentration). Our estimated uncertainty should perhaps be larger than stated for the lower concentration sample.

TABLE II
CONCENTRATION AND MAGNETIC MOMENT OF NATIVE MoFe-PROTEIN

		Sample I	Sample II
[IRON]			
Colorimetric	[Fe]/30 (mM)	0.51	0.27
Atomic absorption	[Fe]/30 (mM)	0.43	0.30
Plasma emission	[Fe]/30 (mM)	0.57(5)*	0.29(3)*
[MOLYBDENUM]			
Atomic absorption	[Mo]/2 (mM)	0.46	0.29
Plasma emission	[Mo]/2 (mM)	0.52(6)*	0.29(4)*
Concentration	c (mM)	0.50(5)‡	0.29(1)‡
Volume	V (ml)	0.180(3)	0.180(3)
Slope	m' (μJ/T · sample)	5.65(9)	2.79(8)
Sample n^2_{eff}	0.537 m'/cV	33.7(35)	28.7(14)
Impurity n^2_{eff}	1.0(2)% Fe^{2+}	7.2(14)	7.1(14)
Difference protein n^2_{eff}	MoFe-protein	26.5(38)	21.6(20)
Average n^2_{eff}	MoFe-protein	24.1(43)	

*Measured uncertainty found using standards prepared by different individuals. This was done for the plasma emission data only.
‡Uncertainty found in averaging the column of five independent observations of protein concentration in this table.

Next we will examine the saturation magnetization of the MoFe-protein (Sample I) shown in Fig. 9. The difference between the MoFe-protein data and the calculated magnetization of the two FeMo-co centers (Fig. 9 *A*, *dashed line*) is given in Fig. 9 *B*. This difference magnetization can be attributed to the ferrous impurity iron observed in the Mössbauer spectra. The solid lines shown in Fig. 9 *B* were calculated assuming the Fe^{2+} impurity (S_I = 2) had zero-field splitting parameters D_I = 3.5 cm^{-1} and E_I/D_I = 0. (Comparable fits were obtained using D_I = 2.5 cm^{-1} with E_I/D_I = ⅓ or using D_I = −2.6 cm^{-1} with E_I/D_I = 0. The subscripts refer to the impurity.) The total impurity in the sample as indicated by this fit was 24 nmol or 0.27 mol per mol protein or 0.9(1)% of the iron in the sample. This is, within uncertainties, the value (1.0(2)%) determined from the high temperature Mössbauer spectrum of this sample. The solid lines of Fig. 9 *A* for the total magnetization at each field were obtained by summing the dashed lines of Fig. 9 *A* for the Fe-Moco centers and the solid lines of Fig. 9 *B* for the impurity magnetization.

Since all the magnetization of the MoFe-protein can be attributed to contributions from FeMo-co centers and ferrous impurity iron, we conclude that no other metal components in native MoFe-protein are paramagnetic. For Sample I, even if we take the lower limits for the FeMo-co

[5] This uncertainty is quite large despite considerable effort to measure the metal concentrations precisely. A total of 16 aliquots of each sample were measured, using three different methods and seven independent series of standards. The preparation of samples for each method was different, thereby minimizing systematic errors. Improvement in this concentration measurement is desirable since it has five times the uncertainty of the Curie slope or sample volume measurements and therefore dominates the uncertainty in the measured value of the magnetic moment. Quantitative analytical techniques, not commonly used in metal analyses of proteins, are required for lower overall uncertainties. Analysis by an outside laboratory will not yet yield more precise results than those reported here.

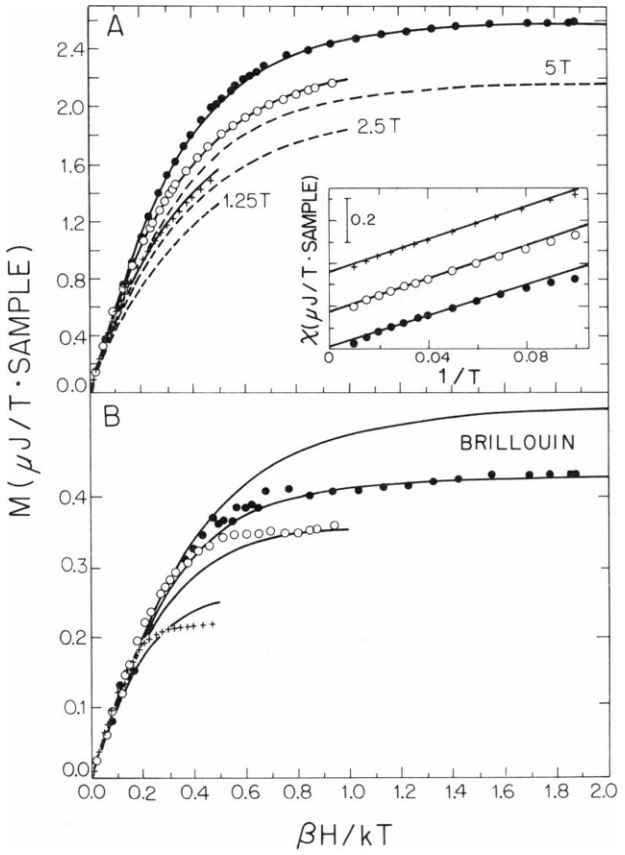

FIGURE 9 (*A*) Magnetization of native MoFe-protein from *A. vinelandii* (Sample I, 180 (3) μl at a concentration of 500(50) μM) at three fixed fields (●, 5 T; ○, 2.5 T; +, 1.25 T) plotted in SI units against $\beta H/kT$. Data were collected for the sample and control and subtracted. This difference data at each field have been translated vertically to bring its intercept to zero. Several of the high temperature data points have been omitted for clarity. The dashed lines are the calculated magnetization at each field for the two FeMo-co centers. These dashed curves were computed using $S_M = \frac{3}{2}$, $D_M = 6.1\ cm^{-1}$, and $E_M/D_M = 0.055$ and assuming a total of 180 nmol of FeMo-co centers in the sample. The solid lines are the sum at each field of the dashed curve of *A* and the solid curve of *B*. The data were collected using the BTi SQUID susceptometer at the National Magnet Laboratory of M.I.T. (*Inset*) The high temperature difference data of native MoFe-protein (Sample I) plotted as sample susceptibility in SI units against inverse temperature. The symbols distinguishing data at each fixed field have the same meaning as in the main figure. The data were analyzed as described in Fig. 8. The results of these fits are tabulated below:

Field	Points included (from left)	Slope
T		*μJ/T sample*
5.000	3–7	5.73
2.500	2–10	5.55
1.250	3–10	5.65

The uncertainty in the slope found by averaging the values measured at each of the three fields is ±1.6%. (*B*) Magnetization of the Fe^{2+} impurity in the native MoFe sample (Sample I) at three fixed fields (●, 5 T; ○, 2.5 T; +, 1.25 T) plotted in SI units against $\beta H/kT$. The experimental points were found by subtracting the calculated magnetization of the FeMo-co centers (*dashed line*) from the points in *A*. The solid lines in *B* were calculated assuming $S_I = 2$, $D_I = 3.5\ cm^{-1}$, and $E_I/D_I = 0$ for the impurity. The amount of impurity spin in the sample determined by this fit is 24 nmol or 0.27 mol impurity per mol protein or 0.9% of the sample's iron.

center and Fe^{2+} impurity contributions there is not enough paramagnetism left to accommodate more than 0.1 mol S-site with spin $S = 1$ per mole of protein. Thus, we conclude that the S-site irons are diamagnetic.

The high temperature data shown in the inset of Fig. 9 *A* are linear up to above 70 K where it begins to be affected by ferromagnetic impurities in the sample holders. That the data obey the Curie law indicates that no excited states having spin different from the ground state have been populated at temperatures up to 70 K for either the FeMo-co centers or the P-clusters.

VI. SUMMARY

New techniques have been developed that extend the sensitivity limit of magnetization studies more than an order of magnitude from a noise level corresponding to a concentration of ~200 μM spin ½ electrons to better than 20 μM. Deuteration of the buffer to remove slowly relaxing protons and careful attention to residual ferromagnetic impurities in sample holders are required to reduce noise to this low level.

The effects of ferromagnetic impurities in sample holders are minimized by collecting data on the sample and its control at fixed high fields (above 0.3 T) over a range of low temperatures (below 70 K) and then subtracting. This difference data are then translated vertically to bring the magnetization intercept to zero. This removes the (constant) magnetization difference due to different levels of ferromagnetic impurities in the two holders. A sealed holder free of these impurities would open the door to routine study at low fields (below 0.3 T) and at high temperatures (above 70 K) and of isotherms.

In principle, the field and temperature dependence of the magnetization of a metalloprotein reveals the spin and the zero-field splitting of its paramagnetic centers and the strength of exchange coupling between its centers. In practice, the major difficulty in extracting this information lies in properly removing the contributions of paramagnetic impurities. One way around this difficulty is to trigger the magnetization change of interest by using a light pulse (9) or by injecting a gas. Subtraction of the data collected before the trigger will remove those impurities not affected by the trigger. When a trigger cannot be used the methodology described in this paper seems to be the best approach. This methodology consists of measuring the level of impurities in the magnetization sample using EPR and Mössbauer spectroscopies and of subtracting a matched control. Even with these techniques, remaining uncertainties in the measured concentrations of high spin impurities often make large contributions to the uncertainty of the final result.

A second practical problem limiting the interpretation of metalloprotein magnetization data is the uncertainty in the measurement of the metal concentration. At present it is possible to measure the Curie law slope of the sample and the volume of the sample each to better than 2%. Metal concentration measurements can have uncertainties substantially larger than ±3%. The resulting uncertainty in the measurement of the magnetic moment is dominated by this large uncertainty in the metal concentration.

It is worth stressing that, in these studies where a well defined Curie slope is observed, there is no need to use the apoprotein in the control to achieve an appropriate diamagnetic reference state. A mismatch in the diamagnetism of the sample and control results only in a constant offset that is easily removed by defining the magnetization intercept of the Curie region of the difference data to be zero. At this point our strategy is to proceed to measure the metalloprotein magnetization on the assumption that a well-defined Curie region will be found in the data. This has turned out to be the case in many of our ongoing studies including several instances where it was not expected to happen. When the presence of exchange coupling in the metalloprotein results in there being no Curie region, other procedures will be required.

In those studies where protein concentration can be reliably measured and where impurities are minimal, as in the study of myoglobin (9), the spin can be determined from the Curie slope and D can be measured from the saturation magnetization at a single field. Further data are not essential and may serve only to verify what is already known. However, we routinely measure three or four isofield curves (at 5, 2.5, 1.25, and 0.625 T) and examine the internal structure of these data for evidence of unexpected magnetic properties of the metalloprotein sample. The high temperature data usually, but not always, yield a field independent slope, indicative of the Curie region. Once the Curie slope is known the intercepts can be set to zero, giving a well-defined family of isofield curves. When these curves lie on top of each other, spin $S = \frac{1}{2}$ is indicated. The form of the saturation curve at 5 T is a sensitive indicator of the spin of the sample. For instance, the first evidence for the spin $S = \frac{3}{2}$ state of the Fe-protein of nitrogenase was the form of its saturation magnetization curve (7). In several of our studies this examination of the form of the data has led us to question (and correct) the measured protein concentration or measured purity of a particular magnetization sample. These techniques have greatly increased the reliability of our interpretation of the magnetization data.

A more sensitive and a faster SQUID susceptometer would be valuable despite these inherent limitations on the interpretation of metalloprotein magnetization data. All of the powerful techniques for studying the magnetic properties of metalloproteins (Mössbauer, EPR, ENDOR, and low temperature MCD spectroscopies) have the disadvantage of requiring frozen samples at cryogenic temperatures. High sensitivity SQUID magnetization techniques have the potential of extending magnetic studies of these same metalloprotein samples to room temperature. Such studies in turn will lay the groundwork for room temperature kinetics studies of metalloproteins using the SQUID susceptometer (34).

A more sensitive SQUID susceptometer would make it possible to reduce protein concentrations of optically dense samples to the point where the samples become transparent. Photo-triggered magnetization experiments are difficult to interpret unless the sample has been uniformly excited. Further improvements in susceptometer sensitivity will not change the inherent difficulties arising from impurity contributions and from uncertainties in the metal concentration but will extend the present quality of information to those optically triggered studies that require lower metalloprotein concentrations.

We thank Dr. John S. Philo for several extremely useful suggestions.

This work has been supported by the United States Department of Agriculture Grant USDA/83-CRCR1-1284 (E. P. Day), by the National Institutes of Health Grants GM32394 (E. P. Day) and GM22701 (E. Münck), and by the National Science Foundation Grant DMR-82-03528 (A. Roy).

Received for publication 12 March 1987 and in final form 8 July 1987.

REFERENCES

1. Day, E. P. 1972. Detection of NMR using a Josephson-junction magnetometer. *Phys. Rev. Lett.* 29:540–542.
2. Roy, A., E. P. Day, and D. M. Ginsberg. 1984. Techniques for reproducibility at the 0.01% level in measurements using a SQUID susceptometer. *Bull. Am. Phys. Soc.* 29:368a. (Abstr.)
3. Turner, E. H., A. M. Sachs, and E. M. Purcell. 1949. Some measurements of nuclear spin-lattice relaxation times in solids. *Phys. Rev.* 76:465–466a. (Abstr.)
4. Palmer, G., W. R. Dunham, J. A. Fee, R. H. Sands, T. Iisuka, and T. Yonetani. 1971. The magnetic susceptibility of spinach ferredoxin from 77–250 K. A measurement of the antiferromagnetic coupling between the two iron atoms. *Biochim. Biophys. Acta.* 245:201–207.
5. Moss, T. H., D. Petering, and G. Palmer. 1969. The magnetic susceptibility of oxidized and reduced ferredoxins from spinach and parsley and the high potential protein from chromatium. *J. Biol. Chem.* 244:2275–2277.
6. Petersson, L., R. Cammack, and K. K. Rao. 1980. Antiferromagnetic exchange interaction in the two-iron-two-sulphur ferredoxin from the blue-green alga *Spirulina maxima* studied with a highly sensitive magnetic balance. *Biochim. Biophys. Acta.* 622:18–24.
7. Lindahl, P. A., E. P. Day, T. A. Kent, W. H. Orme-Johnson, and E. Münck. 1985. Mössbauer, EPR, and magnetization studies of the *Azotobacter vinelandii* Fe-protein: evidence for a $[4Fe\text{-}4S]^{1+}$ cluster with spin $S = \frac{1}{2}$. *J. Biol. Chem.* 260:11160–11173.
8. Savicki, J. P., G. Lang, and M. Ikeda-Saito. 1984. Magnetic susceptibility of oxy- and carbonmonoxyhemoglobins. *Proc. Natl. Acad. Sci. USA.* 81:5417–5419.
9. Roder, H., J. Berendzen, S. F. Bowne, H. Frauenfelder, T. B. Sauke, E. Shyamsunder, and M. B. Weissman. 1984. Comparison of the magnetic properties of deoxy- and photodissociated myoglobin. *Proc. Natl. Acad. Sci. USA.* 81:2359–2363.
10. Philo, J. S., and W. M. Fairbank. 1977. High-sensitivity magnetic

susceptometer employing superconducting technology. *Rev. Sci. Instrum.* 48:1529–1536.

11. Abragam, A., and B. Bleaney. 1970. Electron Paramagnetic Resonance of Transition Ions. Clarendon Press, Oxford. Chapter 3.
12. Davis, L. C., V. K. Shah, W. J. Brill, and W. H. Orme-Johnson. 1972. Nitrogenase II. Changes in the EPR signal of component I (iron-molybdenum protein) of *Azotobacter vinelandii* nitrogenase during repression and derepression. *Biochim. Biophys. Acta.* 256:512–523.
13. Smith, B. E., D. J. Lowe, and R. C. Bray. 1972. Nitrogenase of *Klebsiella pneumoniae*: electron-paramagnetic-resonance studies on the catalytic mechanism. *Biochem. J.* 130:641–643.
14. Münck, E., H. Rhodes, W. H. Orme-Johnson, L. C. Davis, W. J. Brill, and V. K. Shah. 1975. Nitrogenase VIII. Mössbauer and EPR spectroscopy. The MoFe protein component from *Azotobacter vinelandii* OP. *Biochim. Biophys. Acta.* 400:32–53.
15. Zimmermann, R., E. Münck, W. J. Brill, V. K. Shah, M. T. Henzl, J. Rawlings, and W. H. Orme-Johnson. 1978. Nitrogenase X: Mössbauer and EPR studies on reversibly oxidized MoFe protein from *Azotobacter vinelandii* OP. Nature of the iron centers. *Biochim. Biophys. Acta.* 537:185–207.
16. Huynh, B. H., E. Münck, and W. H. Orme-Johnson. 1979. Nitrogenase XI: Mössbauer studies on the cofactor centers of the MoFe protein from *Azotobacter vinelandii* OP. *Biochim. Biophys. Acta.* 576:192–203.
17. Huynh, B. H., M. T. Henzl, J. A. Christner, R. Zimmermann, W. H. Orme-Johnson, and E. Münck. 1980. Nitrogenase XII. Mössbauer studies of the MoFe protein from *Clostridium pasteurianum* W5. *Biochim. Biophys. Acta.* 623:124–138.
18. Venters, R. A., M. J. Nelson, P. A. McLean, A. E. True, M. A. Levy, B. M. Hoffman, and W. H. Orme-Johnson. 1986. ENDOR of the resting state of nitrogenase molybdenum-iron proteins from *Azotobacter vinelandii, Klebsiella pneumoniae,* and *Clostridium pasteurianum:* ^{1}H, ^{57}Fe, ^{95}Mo, and ^{33}S studies. *J. Am. Chem. Soc.* 108:3487–3498.
19. Kunze, R. K., Jr., and E. P. Day. 1980. The temperature dependence of the diamagnetism of liquids. *J. Chem. Phys.* 72:5809–5814.
20. Petersson, L., and A. Ehrenberg. 1985. Highly sensitive Faraday balance for magnetic susceptibility studies of dilute protein solutions. *Rev. Sci. Instrum.* 56:575–580.
21. Tweedle, M. F., L. J. Wilson, L. Garcia-Iñiguez, G. T. Babcock, and G. Palmer. 1978. Electronic state of heme in cytochrome oxidase III. The magnetic susceptibility of beef heart cytochrome oxidase and some of its derivatives from 7–200 K. Direct evidence for an antiferromagnetically coupled Fe(III)/Cu(II) pair. *J. Biol. Chem.* 253:8065–8071.
22. Redfield, A. G., and C. Moleski. 1972. Vibrating sample magnetometer for protein research. *Rev. Sci. Instrum.* 43:760–762.
23. Moss, T. H. 1978. Magnetic susceptibility applied to metalloproteins. *Methods Enzymol.* 54:379–396.
24. Cabrera, B. 1975. The use of superconducting shields for generating ultra-low magnetic field regions and several related experiments. Ph.D. thesis, Stanford University.
25. Morrish, A. H. 1965. The Physical Principles of Magnetism. John Wiley & Sons, Inc., New York. 360–363.
26. Roy, A. 1984. 3d magnetic dopant atoms in transition-metal superconductors: Part I. Localized magnetic moments on chromium and manganese dopant atoms in niobium and vanadium. Part II. The effects of chromium and manganese dopant atoms on the upper critical magnetic field of niobium. Ph.D. thesis, University of Illinois.
27. Orme-Johnson, W. H. 1985. Molecular basis of biological nitrogen fixation. *Annu. Rev. Biophys. Biophys. Chem.* 14:419–459.
28. Burgess, B. K. 1984. Structure and reactivity of nitrogenase—an overview. *In* Advances in Nitrogen Fixation Research. C. Veeger and W. E. Newton, editors. Nijhoff/Junk, The Hague, Netherlands. 103–113.
29. Hausinger, R. P., and J. B. Howard. 1982. The amino acid sequence of the nitrogenase iron protein from *Azotobacter vinelandii. J. Biol. Chem.* 257:2483–2487.
30. Smith, J. P., M. H. Emptage, and W. H. Orme-Johnson. 1982. Magnetic susceptibility studies of native and thionine-oxidized molybdenum-iron protein from *Azotobacter vinelandii* nitrogenase. *J. Biol. Chem.* 257:2310–2313.
31. Shah, V. K., and W. J. Brill. 1977. Isolation of an iron-molybdenum cofactor from nitrogenase. *Proc. Natl. Acad. Sci. USA.* 74:3249–3253.
32. Fisher, D. S., and D. C. Price. 1964. A simple serum iron method using the new sensitive chromogen tripyridyl-s-triazine. *Clin. Chem.* 10:21–31.
33. Dahlquist, R. L., and J. W. Knoll. 1978. Inductively coupled plasma-atomic emission spectrometry—analysis of biological materials and soils for major, trace, and ultra-trace elements. *Appl. Spectros.* 32:1–30.
34. Philo, J. S. 1977. Kinetics of hemoglobin-carbon monoxide reactions measured with a superconducting magnetometer: a new method for fast reactions in solution. *Proc. Natl. Acad. Sci. USA.* 74:2620–2623.